FEBS Letters 430 (1998) 370–376 FEBS 20458

Single mutations strongly alter the K^+-selective pore of the K_{in} channel KAT1

Ingo Dreyer[a], Dirk Becker[a], Monica Bregante[b], Franco Gambale[b], Michaela Lehnen[c], Klaus Palme[c], Rainer Hedrich[a,*]

[a] *Julius-von-Sachs-Institut für Biowissenschaften, Lehrstuhl Botanik I-Molekulare Pflanzenphysiologie und Biophysik, Julius-von-Sachs-Platz 2, D-97082 Würzburg, Germany*
[b] *Istituto di Cibernetica e Biofisica, CNR, Via de Marini 6, I-16149 Genoa, Italy*
[c] *Max-Delbrück-Laboratorium in der Max-Planck-Gesellschaft, Carl-von-Linne-Weg 10, D-50829 Cologne, Germany*

Received 6 April 1998; revised version received 28 May 1998

Abstract Voltage-dependent potassium uptake channels represent the major pathway for K^+ accumulation underlying guard cell swelling and stomatal opening. The core structure of these *Shaker*-like channels is represented by six transmembrane domains and an amphiphilic pore-forming region between the fifth and sixth domain. To explore the effect of point mutations within the stretch of amino acids lining the K^+ conducting pore of KAT1, an *Arabidopsis thaliana* guard cell K_{in} channel, we selected residues deep inside and in the periphery of the pore. The mutations on positions 256 and 267 strongly altered the interaction of the permeation pathway with external Ca^{2+} ions. Point mutations on position 256 in KAT1 affected the affinity towards Ca^{2+}, the voltage dependence as well as kinetics of the Ca^{2+} blocking reaction. Among these T256S showed a Ca^{2+} phenotype reminiscent of an inactivation-like process, a phenomenon unknown for K_{in} channels so far. Mutating histidine 267 to alanine, a substitution strongly affecting C-type inactivation in *Shaker*, this apparent inactivation could be linked to a very slow calcium block. The mutation H267A did not affect gating but hastened the Ca^{2+} block/unblock kinetics and increased the Ca^{2+} affinity of KAT1. From the analysis of the presented data we conclude that even moderate point mutations in the pore of KAT1 seem to affect the pore geometry rather than channel gating.

Key words: Gating; Inactivation; Pore structure; Site-directed mutagenesis; Voltage-dependent block

1. Introduction

Voltage-gated inwardly rectifying K^+ channels (K_{in} channels) play a fundamental role in plant physiology. These transporters allow plant cells to take up large quantities of potassium essential for cell growth and differentiation. The molecular cloning of plant K_{in} channels and the functional expression in heterologous expression systems provided the basis to relate structural motifs within the channel protein to distinct functions [1–15]. From the gating characteristics, kinetics, pharmacology, and the primary structure, K_{in} channels were grouped within a separate family of voltage-dependent potassium channels [2]. Based on the putative secondary structure with six transmembrane-spanning domains (S1–S6) and a pore region (P) between S5 and S6 (cf. [16] and references therein), plant K_{in} channels resemble voltage-gated outwardly rectifying animal K^+ channels of the *Shaker* type (K_V channels, for review see [17]). In contrast K_{in} channels do not activate at positive but at negative potentials and thus in vivo and in vitro predominantly mediate inward currents. These inward currents do not inactive even during sustained hyperpolarization (see [18] and references therein).

Like K_V channels K_{in} channels represent multisubunit proteins. When expressed in *Xenopus* oocytes plant K_{in} channel α-subunits assemble non-selectively among channel subtypes originating from different tissues, plant species and even different families [19]. An assembly region in the cytoplasmic C-terminal part of the protein has been identified as an essential element for subunit aggregation. This region is highly conserved among different subfamilies of plant K_{in} channels [20]. Similar findings were recently reported for the rat ether-à-go-go potassium channel, an animal K^+ channel with a high degree of homology to K_{in} channels [21].

Due to the structural similarity to K_V channels, differences in assembly and opposite gating, K_{in} channels represent a unique target for studies on the difference between structure and function within *Shaker*-related K^+ channel families. The two K_{in} channels, KST1 from *Solanum tuberosum* [10] and KAT1 from *Arabidopsis thaliana* [1], advanced to a model system for these studies. For both proteins it has recently been shown that the positively charged S4 segment together with the N- and C-termini contribute to the gating of K_{in} channels [19,22,23]. However, the pore region seems to play an extraordinary role, because this domain, besides its function as the permeation pathway [24–27], very likely interacts with the gating machinery as well [22,24,28].

In this study we investigated the influence of point mutations in the pore region of KAT1 on the pore geometry and related it to the crystal structure of the K^+ channel from *Streptomyces lividans* KcsA [29]. Probing the interaction between pore mutants and Ca^{2+} ions we were able to distinguish the effects of the divalent cation on permeation and gating.

2. Materials and methods

2.1. Electrophysiology

Experiments were performed on RNA-injected, voltage-clamped *Xenopus* oocytes using a two-electrode voltage clamp approach as previously described by Hedrich et al. [8]. Because some channel properties of K_{in} channels differ with the expression level [5,7], oocytes with similar K^+ current amplitudes were selected for analysis only.

2.1.1. Solutions. Experiments were performed either in 30 mM or in 10 mM KCl, 10 mM MES/Tris, pH 5.6. Various molar fractions of 30 mM between $CaCl_2$ and $MgCl_2$ were used to maintain the ionic strength. All solutions were adjusted to 220 mosmol/kg with sorbitol.

*Corresponding author.
E-mail: hedrich@botanik.uni-wuerzburg.de

PII: S0014-5793(98)00694-2

2.2. Biophysical analysis

2.2.1. Ion blockTo obtain the instantaneous current-voltage characteristic of the open channel ($I_T(V)$) the membrane voltage after approaching steady-state activation at $V=-150$ mV was stepped to various values. $I_T(V)$ relationships were deduced from extrapolating the tail current onset to $t=0$.

Current-voltage relationships of tail and steady-state currents in the presence of an antagonist were fitted according to the Woodhull model [30]:

$$I(V) = I^0(V)\frac{1}{1+\frac{[Ca^{2+}]^n}{\kappa}e^{-\left(\frac{zF}{RT}\delta V\right)}}$$

$$= I^0(V)\frac{1}{1+e^{-\left(\frac{zF}{RT}\delta(V-V_{Block1/2})\right)}} \quad (1)$$

where F, R, and T have their usual meanings. $I^0(V)$ denotes the current in the absence of the blocking ion, z its valence, δ the fraction of the transmembrane voltage sensed by the ion, $[Ca^{2+}]$ the blocker concentration, n the stoichiometry coefficient of the blocking reaction, and κ the K_i at 0 mV. κ is correlated with the energy which characterizes the affinity of the Ca^{2+} binding site (ΔG_B; Fig. 6C) Comparing two mutants characterized by κ_1 or ΔG_{B1} and κ_2 or ΔG_{B2} the difference

$$\ln\kappa_1-\ln\kappa_2 = \frac{1}{kT}(\Delta G_{B2}-\Delta G_{B1}) = \frac{1}{kT}\cdot\Delta G_{aff} \quad (2)$$

is a measure for the altered affinity to the blocking ion ΔG_{aff}.

Given a $[Ca^{2+}]$ value, the half-blocking voltage $V_{Block1/2}$ could be obtained from $I(V_{Block1/2}) = 1/2\ I^0(V_{Block1/2})$. From Eq. 1 it can be deduced:

$$\ln[Ca^{2+}] = \frac{zF}{RT}\frac{\delta}{n}V_{Block1/2} + \frac{1}{n}\ln\kappa \quad (3)$$

i.e. in a $\ln[Ca^{2+}]$-$V_{Block1/2}$ plot the slope is a measure for the voltage dependence of the block, and

$$\ln\frac{I^0-I}{I} = n\ln[Ca^{2+}]-\ln\kappa-\frac{zF}{RT}\delta V \quad (4)$$

i.e. in a $\ln[(I^0\text{-}I)/I]$-$\ln[Ca^{2+}]$ plot the slope is a measure for the concentration dependence of the block (stoichiometry coefficient n).

Combining Eqs. 2 and 3 the difference in the affinity energy can be calculated by

$$\Delta G_{aff} = kT\cdot\left(\frac{zF}{RT}\cdot(\delta_2 V^2_{Block1/2}-\delta_1 V^1_{Block1/2}) + (n_1-n_2)\cdot\ln[Ca^{2+}]\right) \quad (5)$$

2.3. Molecular biology

KAT1 single mutants were generated as previously described [24]. To construct the double mutants T256E/H267A and T256S/H267A the single mutants KAT1-T256E, KAT1-T256S, and KAT1-H267A in pGEMHE [31] were incubated with the restriction enzymes *Dsa*I and *Sal*I which resulted in the release of two fragments, one 800 bp fragment covering position 256 and a 4600 bp fragment representing the expression vector as well as the other parts of the KAT1 sequence including position 267. The 800 bp fragments containing the T256E and T256S mutations were isolated and ligated into the 4600 bp backbone of the KAT1-H267A restriction digest. The double mutants were verified by sequencing.

3. Results

3.1. Low-affinity Ca^{2+} block in KAT1 wild-type

In previous experiments performed in 30 mM K^+ in the bath, Ca^{2+} concentrations up to 30 mM, and voltages in the range of −170 mV to +20 mV no Ca^{2+} sensitivity of the KAT1 wild-type could be detected [24]. A recent study, however, showed that in guard cell protoplasts the degree of the voltage-dependent Ca^{2+} block of plasma membrane K^+_{in} channels increased when lowering the external K^+ concentration. In *Vicia faba* for example the Ca^{2+} block in media containing 20 mM Ca^{2+} in addition to 30 mM K^+ was comparable to the block in solutions based on 10 mM K^+ and 1 mM Ca^{2+} [32]. We therefore tested the Ca^{2+} sensitivity of KAT1 expressed in *Xenopus* oocytes in the presence of 10 mM K^+ only. Using Ca^{2+} concentrations up to 30 mM a divalent block was resolved at voltages negative of −200 mV (Fig. 1A). With more hyperpolarizing voltages the strength of the block increased. In this voltage range a weak Ca^{2+} block could be observed in media containing 30 mM K^+ and 30 mM Ca^{2+} as well (Fig. 1B). Thus the KAT1 wild-type channel when expressed in *Xenopus* oocytes exhibits a very low Ca^{2+} susceptibility, only.

3.2. Mutations at position T256 modify the Ca^{2+} sensitivity of KAT1

In the following we tested whether and in which way single site mutations within the pore of KAT1 modify the interaction with the divalent blocker. Since in a previous study [24] we observed that a pore mutant on position 256, T256E, is more sensitive to extracellular Ca^{2+} than the KAT1 wild-type

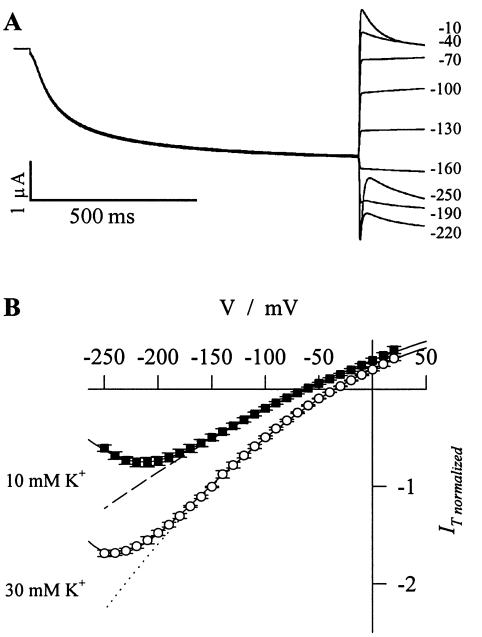

Fig. 1. Low affinity Ca^{2+} block in the K_{in} channel KAT1 expressed in *Xenopus* oocytes. Low affinity Ca^{2+} block was uncovered using a two step pulse protocol. The first pulse to −150 mV activated KAT1 channels but not oocyte-intrinsic channels. At the beginning of the second 300-ms pulse the driving force for the ions was altered while the open probability of KAT1, and oocyte-intrinsic channels remained unaffected. A: Representative current families from KAT1-expressing oocytes measured in 10 mM K^+/30 mM Ca^{2+}. Voltages of the second pulse are indicated in mV. B: Instantaneous current-voltage characteristics of the KAT1 wild-type measured in 10 mm K^+/1 mM Ca^{2+} (dashed line), 10 mM K^+/30 mM Ca^{2+} (closed squares), 30 mM K^+/1 mM Ca^{2+} (dotted line), and 30 mM K^+/30 mM Ca^{2+} (open circles). Solid lines represent best fits according to Eq. 1. This yielded $\delta = 0.43\pm0.03$, $V_{Block1/2}{}^{10mMK} = -250.1\pm1.8$ mV, and $V_{Block1/2}{}^{30mMK} = -280.2\pm1.8$ mV. Currents in B were normalized to $I(-150$ mV, 30 mM K^+/1 mM $Ca^{2+}) = -1$. Each data point represents the mean of three or four measurements. Error bars indicate the standard deviation.

we focused on this residue and further created the mutants T256D, T256H, T256K, T256Q, T256M, T256I, and T256S.

The substitution T256E increased the Ca^{2+} affinity of KAT1 by at least $\Delta G_{aff} \geq 6\ kT$ (Fig. 2A, left; Fig. 3; Table 1; Eq. 5). To prove whether this gain in sensitivity results from the negative charge introduced, we altered the charge density at that position by the mutations T→D, T→H, T→K, and T→Q. In line with previous observations the mutant T256D exhibited a pronounced Rb^+ permeability when compared to wild-type KAT1 [25]. However, in 30 mM K^+ and even in 100 mM K^+ the current amplitudes were too small to allow reliable Ca^{2+} interaction studies. From similar experiments we deduced that residues with large and positively charged side chains like histidine or lysine at position 256, T256H and T256K, seemed to hinder K^+ fluxes through the channel.

In contrast to T256E the mutant channel T256Q did not show an increase in Ca^{2+} sensitivity (not shown). This finding seemed to indicate that the negative charge in T256E is responsible for the pronounced Ca^{2+} block. The exchange of the hydrophilic polar threonine by amino acids with hydrophobic non-polar side chains (isoleucine and methionine), however, increased the Ca^{2+} sensitive of the channels as well. Similar to T256E, the mutant T256M was blocked by extracellular calcium in a voltage-dependent manner (Fig. 3A). The interaction of the open pore of both mutant channels, T256M and T256E, with the Ca^{2+} ion could be described with the Woodhull model [30]. δ values of 0.32 for T256E and 0.55 for T256M indicate that the blocking ion might move 32% and 55%, respectively, along the voltage drop across the selectivity filter. The block in the mutant T256M was, however, weaker than in T256E. This distinction could be expressed by the difference in the affinity energy, $\Delta G_{aff} \approx 4.6\ kT$ (Table 1, Eq. 5), on one hand, and by the inhibitory constant K_i (−150 mV), on the other. In the presence of 30 mM K^+ in the bath, 14.5 mM Ca^{2+} was sufficient to inhibit the K^+

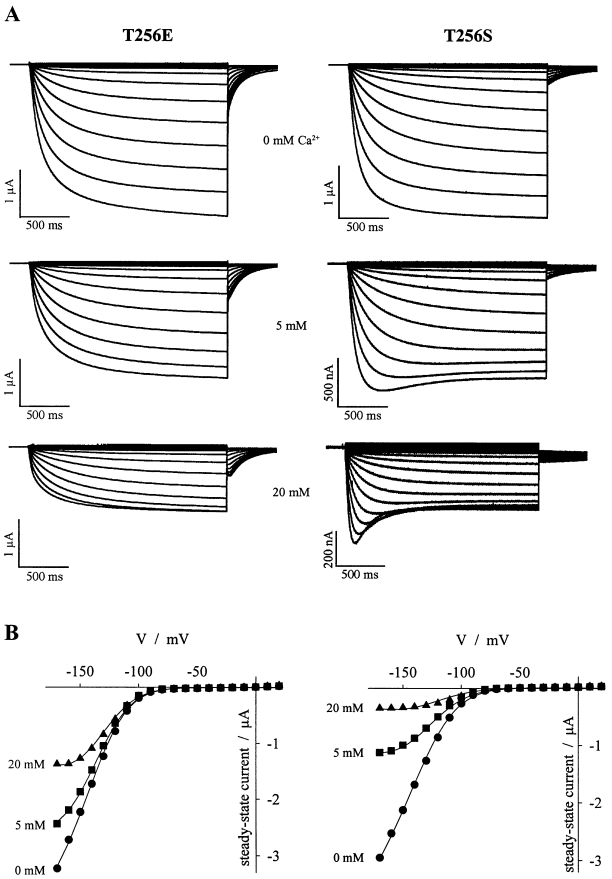

Fig. 2. Ca^{2+} modulation of inward potassium currents in the KAT1 mutants T256E (left) and T256S (right). A: Representative current families from oocytes measured in 30 mM K^+ and 0 mM (top), 5 mM (middle), and 20 mM Ca^{2+} (bottom) respectively. From a holding potential of −20 mV currents were elicited by 1-s voltage steps from −20 mV to −170 mV (10 mV steps) followed by a voltage step to −70 mV. B: Steady-state current-voltage characteristics for the oocytes shown in A. The symbols correspond to Ca^{2+} concentrations of 0 mM (circles), 5 mM (squares), and 20 mM (triangles) in bath. Solid lines represent best fits according to Eq. 1 ($\delta_{T256E} = 0.32 \pm 0.02$, $V_{Block1/2,\ T256E}{}^{5Ca} = -214.3 \pm 2.9$ mV, $V_{Block1/2,\ T256E}{}^{20Ca} = -160.1 \pm 0.8$ mV, $\delta_{T256S} = 0.24 \pm 0.01$, $V_{Block1/2,\ T256S}{}^{5Ca} = -144.4 \pm 1.2$ mV, and $V_{Block1/2,\ T256S}{}^{20Ca} = -68.0 \pm 5.3$ mV).

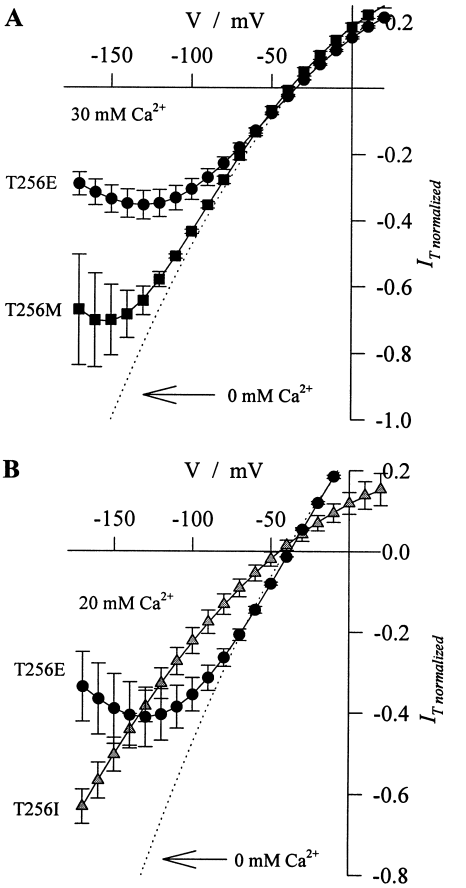

Fig. 3. Voltage-dependent and voltage-independent Ca^{2+}-block of KAT1-T256 mutants in 30 mM K^+. A: Instantaneous current-voltage characteristics of the mutants T256E (closed circles) and T256M (closed squares) measured in 30 mM Ca^{2+}. B: Instantaneous current-voltage characteristics of the mutants T256E (closed circles) and T256I (gray triangles) measured in 20 mM Ca^{2+}. The dotted lines indicate the current-voltage characteristics in the absence of Ca^{2+}. Solid lines represent best fits according to Eq. 1. This yielded in A $\delta_{T256E} = 0.32 \pm 0.03$, $V_{Block1/2}{}^{T256E} = -124.6 \pm 12.4$ mV, $\delta_{T256M} = 0.47 \pm 0.14$, $V_{Block1/2}{}^{T256M} = -174.7 \pm 6.0$ mV, and in B $\delta_{T256E} = 0.32 \pm 0.06$, $V_{Block1/2}{}^{T256E} = -133.5 \pm 19.6$ mV. The data for T256I were fitted according to the equation $I(V) = a \cdot I^0(V)$, $a = 0.51 \pm 0.01$. Currents were normalized to $I(-150$ mV, 0 mM $Ca^{2+}) = -1$. Each data point represents the mean of three or four measurements. Error bars indicate the standard deviation.

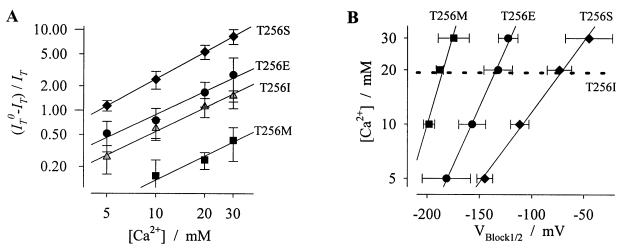

Fig. 4. Ca^{2+} inhibition of the K^+ currents in the KAT1 mutants T256E (circles), T256I (gray triangles), T256M (squares), and T256S (rhombi). Each data point represents the mean of three to ten measurements. Error bars indicate the standard deviation. A: Concentration dependence of the Ca^{2+} block displayed in a $\ln[I^0-I]$-$\ln[Ca^{2+}]$ plot. Data were generated at −150 mV. Solid lines represent best fits according to Eq. 4 ($n_{T256E} = 1.0 \pm 0.3$, $n_{T256M} = 1.0 \pm 0.1$, $n_{T256M} = 1.0 \pm 0.3$, and $n_{T256S} = 1.1 \pm 0.1$. B: Voltage dependence of the Ca^{2+} block displayed in a $\ln[Ca^{2+}]$-$V_{Block1/2}$ plot. Solid lines represent best fits according to Eq. 3. The dashed line indicates the voltage-independent Ca^{2+} block in the mutant T256I.

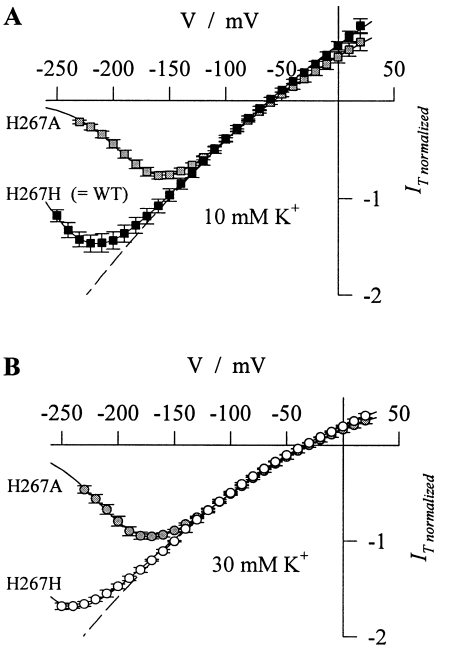

Fig. 5. The mutation of the highly conserved histidine in the GYGDxx**H** motif to alanine alters the affinity of KAT1 to Ca^{2+}. A: Instantaneous current-voltage characteristics of the KAT1 wild-type (closed squares) and the mutant KAT1-H267A (gray squares) measured in 10 mM K^+/30 mM Ca^{2+}. B: Instantaneous current-voltage characteristics of the KAT1 wild-type (open circles) and the mutant KAT1-H267A (gray circles) measured in 30 mM K^+/30 mM Ca^{2+}. The dashes lines indicate the current-voltage characteristics in 1 mM Ca^{2+}. Solid lines represent best fits according to Eq. 1. The data for the wild-type are presented in Fig. 1. The fits for H267A yielded $\delta_{10K} = 0.55 \pm 0.02$, $V_{Block1/2}{}^{10K} = -178.1 \pm 2.2$ mV, $\delta_{30K} = 0.52 \pm 0.02$, and $V_{Block1/2}{}^{30K} = -200.1 \pm 1.5$ mV. Currents were normalized to $I(-150$ mV, 1 mM $Ca^{2+}) = -1$. Each data point represents the mean of three or four measurements. Error bars indicate the standard deviation.

current through the mutant channel T256E by ∼50% while in T256M even in 30 mM Ca^{2+} a related blocking efficiency could not be achieved (Fig. 3A, Table 1). Like the K^+ channel mutants T256E and T256M, K^+ currents through KAT1-T256I were inhibited by Ca^{2+} as well. The Ca^{2+} block of the latter, however, characterized by a K_i of ∼19 mM (Table 1), was voltage-*in*dependent (Fig. 3B). Despite these large differences in sensitivity and voltage dependence of the Ca^{2+} block the mutants T256E, T256I, and T256M, a stoichiometry coefficient of $n \approx 1$ suggests that in all three mutants one Ca^{2+} ion occludes one channel (Fig. 4A, Table 1). Thus the Ca^{2+} block in T256E, T256I, and T256M is based on similar molecular mechanisms.

3.3. Does the mutant T256S inactivate?

In plant K_{in} channels in vivo and after heterologous expression of wild type and mutant channels inactivation has not been observed so far. The mutant T256S, however, which differs from the wild-type in a single methyl group, exhibited an inactivation-like behavior (Fig. 2A, right, lower traces). During a 2-s hyperpolarizing voltage pulse the current amplitude initially increased, before it slowly decreased. This apparent 'inactivation' was reminiscent of C-type inactivation in the *Shaker* channel [33,34] or P-type inactivation in Kv2.1 [35], processes caused by conformational changes of the outer pore. The rate of inactivation was dependent on the extracellular cation concentrations. When we increased the amount of Ca^{2+} the inactivation process speeded up. During voltage pulses to −150 mV the time course of the current decay followed a single exponential with a time constant $\tau = 946 \pm 203$ ms in 5 mM, $\tau = 555 \pm 184$ ms in 10 mM, $\tau = 248 \pm 40$ ms in 20 mM, and $\tau = 181 \pm 34$ ms in 30 mM Ca^{2+} ($n = 3$–5). With

Table 1
Characteristics of the Ca^{2+} phenotype of KAT1 mutants

		δ	K_i at −150 mV (mM)	$V_{Block1/2}$ 30 mM Ca^{2+} (mV)	Stoichiometry coefficient	Block kinetics
KAT1 WT 10 mM K^+		0.45 ± 0.08	> 30	< −250	n.d.	fast
T256E		0.32 ± 0.03	14.5 ± 6.3	−123 ± 9	1.0	fast
T256I		0	19.3 ± 6.9	–	1.0	–
T256M		0.55 ± 0.03	> 30	−175 ± 15	1.0	fast
T256S		0.27 ± 0.03	4.8 ± 0.8	−45 ± 23	1.1	slow
H267A	10 mM K^+	0.55 ± 0.01	> 30	−176 ± 3	n.d.	very fast
	30 mM K^+	0.52 ± 0.02	> 30	−201 ± 3	n.d.	very fast
T256E/H267A		n.d.	n.d.	n.d.	n.d.	very fast
T256S/H267A		0.23 ± 0.03	4.3 ± 0.7	−38 ± 28	1.1	medium

Susceptibility to block by Ca^{2+} ions in 30 mM KCl is given by the inhibition constant K_i at −150 mV. The electrical distance, δ, and half-blocking voltage, $V_{Block1/2}$, were determined according to Eq. 1 for each cell and the stoichiometry coefficient from the linear regression of the $\ln[(I^0-I)/I]$-$\ln[Ca^{2+}]$ plot (Fig. 4A, Eq. 3) for all data. K_i values were determined from interpolating the fits in $\ln[Ca^{2+}]$-$V_{Block1/2}$ plots (cf. Fig. 4B, Eq. 3) to $V_{Block1/2} = -150$ mV.
Data represent the mean of 3–5 measurements ± S.D.

increasing hyperpolarization τ decreased by a factor of 1.5 for a 10-mV change. A similar effect was obtained by lowering the extracellular K^+ concentration to 10 mM. This reduction in the monovalent cation concentration accelerated the apparent inactivation two-fold ($\tau_{10mMK} = 416 \pm 85$ ms, $n = 4$, instead of $\tau_{30mMK} = 946 \pm 203$ ms). Likewise the time course of the C-type inactivation in the *Shaker* channel was slowed when the external K^+ concentration was increased. Alterations in the Ca^{2+} concentration, however, did not affect inactivation kinetics of this channel [34]. Additionally, the inactivation process in *Shaker* was voltage-independent [33,36], while the current decay for the mutant KAT1-T256S shown here was strongly dependent on voltage. At −110 mV, for instance, no inactivation was seen whereas the K^+ current decayed with increasing hyperpolarization. When analyzing the steady-state current-voltage characteristics of the mutant T256S (Fig. 2B) with Eq. 1, the strong Ca^{2+} interaction could be described by the block parameters $\delta \approx 0.27$ and $n \approx 1$ (Fig. 4). The apparent inactivation in the mutant T256S might therefore result from a very slow Ca^{2+} block rather than C-type inactivation.

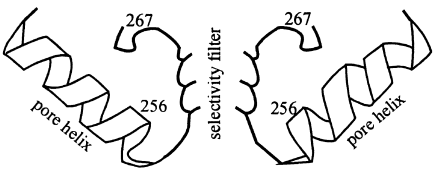

Fig. 7. Model of the inner pore region of the plant K_{in} channel KAT1. The model is based on the crystal structure obtained from the *Streptomyces lividans* channel KcsA [29] and a model designed for the *Shaker* channel [16]. From the four subunits building a functional channel [20], subunits one and three are displayed only. The numbers indicate the positions of the related residues.

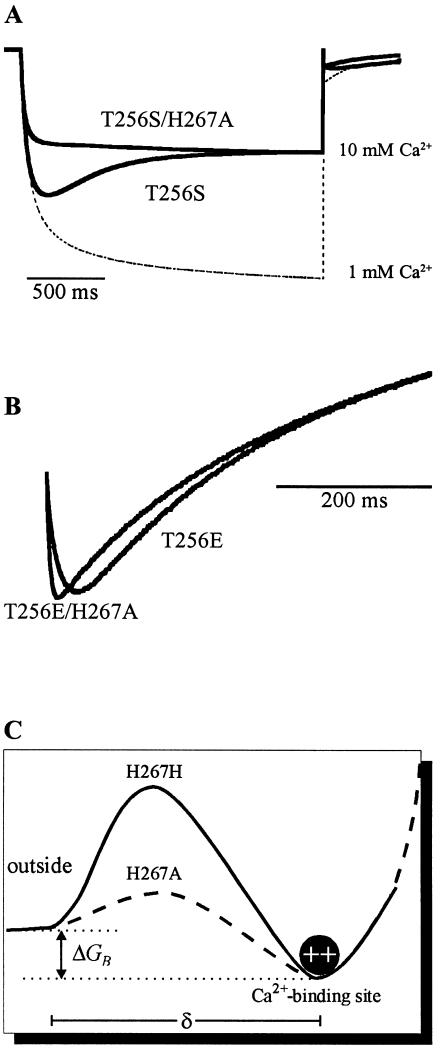

Fig. 6. Effect of H267 on the Ca^{2+} sensitivity of T256E and T256S. A: Elimination of the apparent inactivation due to the mutation H267A. Comparison of potassium currents mediated by T256S and T256S/H267A. Currents were elicited by 2-s activation pulses to −150 mV, measured in 30 mM K^+, 10 mM Ca^{2+}, pH 5.6, and normalized to the steady-state current. To visualize the inhibitory effect of Ca^{2+} the related current trace measured in 1 mM Ca^{2+} in T256S was superimposed. B: Acceleration of the Ca^{2+} unblock in T256E/H267A compared to T256E. Unblocking kinetics were resolved at a potential of −110 mV following an activation pulse to −150 mV (cf. [24]). Currents were measured in 30 mM Ca^{2+} and normalized to peak and steady-state values. C: Cartoon of the energetic profile sensed by the blocking Ca^{2+} ion in H267H (KAT1 wild-type) and H267A. The model is based on Eyring rate theory [37]. δ indicates the depth of the binding site in the transmembrane electrical field.

3.4. Does H267 represent the initial Ca^{2+} barrier?

In order to unequivocally distinguish between Ca^{2+} block and C-type inactivation we replaced the histidine 267 by alanine. The position KAT1-H267 is equivalent to *Shaker*-T449. Changes of this residue strongly affect C-type inactivation in the *Shaker* channel. The substitution T449H slows C-type inactivation while T449A accelerates this process [34]. KAT1-H267A, however, showed neither any kind of inactivation nor any other significant change in the gating behavior, but altered pharmacological properties. The mutation H267A increased the Ca^{2+} sensitivity of KAT1 by at least $\Delta G_{aff} \geq 1.3$ *kT* (Fig. 5A,B, Table 1, Eq. 5), while the voltage dependence of the block showed no significant difference. Similar to wild-type KAT1 the obstructing cation might move 52% along the voltage drop across the selectivity filter.

In order to test the effect of the mutation H267A on the apparent inactivation in the channel KAT1-T256S we created the double mutant T256S/H267A and tested its interaction with calcium ions. Although this channel was still Ca^{2+}-sensitive, in contrast to T256S, no inactivation-like behavior was detectable (Fig. 6A). Instead, the Ca^{2+} sensitivity of T256S/H267A showed all characteristics of a voltage-dependent block with parameters similar to those obtained for the single mutant T256S, $\delta \approx 0.23$ and $n \approx 1$. The apparent inactivation in the mutant T256S thus very likely results from a very slow Ca^{2+} block. Since in this channel the block was *slower* than channel activation an inactivation phenotype was mimicked. The substitution H → A on position 267 seemed to accelerate the interaction of the Ca^{2+} ion with the pore. In the double mutant T256S/H267A the blocking reaction was *faster* than channel activation so that the blocking process could be resolved during deactivation only (cf. [24]). In line with this hypothesis the voltage-dependent Ca^{2+} unblock in the double mutant T256E/H267A was five times as fast as in T256E (Fig. 6A; in 30 mM K^+/30 mM Ca^{2+} at −110 mV: $\tau_{T256E/H267A} = 4.6 \pm 0.8$ ms vs. $\tau_{T256E} = 23.7 \pm 2.2$ ms, $n = 3$). Thus in KAT1 channels carrying the mutation H267A the entry of the blocking Ca^{2+} ions into the pore was facilitated.

4. Discussion

In this study we examined structural motifs affecting the Ca^{2+} sensitivity of the K_{in} channel KAT1. Based on previous observations that mutations of the pore residues L251, T259, and T260 do not markedly alter the affinity of KAT1 to Ca^{2+} [24], we focused on positions T256 and H267. The related channel mutants exhibited a broad variety of Ca^{2+} phenotypes. Point mutations on position 256 affected the affinity for Ca^{2+}, the voltage dependence as well as kinetics of the blocking reaction. Whereas a non-conserved substitution, T256Q, did not influence these parameters, the conserved exchange T256S created a phenotype reminiscent of an inactivation-like behavior. Detailed experiments on the mutants T256S and T256S/H267A, however, indicate that this apparent inactivation originates from a very slow Ca^{2+} block. Moreover, the replacement of histidine by alanine right next to the selectivity filter (GYGDxx**H** motif) neither created inactivation nor fundamentally influenced the gating behavior of the channel.

From the presented data we conclude that the pore histidine which is highly conserved among K_{in} channels [28] serves as a first barrier for Ca^{2+} ions in entering the pore. This conclusion could be explained by a simple model based on the Eyring rate theory (Fig. 6C, [37]). To enter the binding site the Ca^{2+} ion has to cross an energy barrier. The rate of this reaction is inversely correlated with the height of the barrier, i.e. a high barrier implies low rate constants. Supposing that the histidine represents a high barrier and the alanine a low barrier, the model would account for faster blocking and unblocking reactions in the double mutants T256E/H267A and T256S/H267A due to the facilitated entry of Ca^{2+} ions. The height of the barrier in KAT1-H267H (wild-type) compared to the mutant KAT1-H267A, however, cannot explain the difference in Ca^{2+} sensitivity between the mutants T256Q, T256E, T256M, T256S, and T256I. In the mutant channel T256M the obstructing Ca^{2+} ion senses $\sim$55% of the voltage drop indicating a Ca^{2+} binding site deep in the pore. In T256E and T256S this interaction site locates less deep in the pore and in T256I it is even in the periphery. We therefore propose several Ca^{2+} interaction sites within the pore. Consequently the side chain at residue 256 might not represent the interaction site itself but affect the pore geometry. From the lack of correlation between the pattern of the Ca^{2+} sensitivity and the chemical properties as well as size of the side chain one would not expect this residue to line the pore.

In order to further explain our results on the molecular level we adapted the KAT1 sequence to the crystal structure of the pore of the potassium channel KcsA from *Streptomyces lividans* [29]. As shown in Fig. 7 the residue on position 256 appeared to be a component of the pore helix. In KcsA this tilted pore helix provides a rigid backbone which holds the selectivity filter. According to this model alterations of the side chain at position 256 could change the electrostatic and van der Waals interactions of the amino acids in the narrow pore. This in turn would alter the electrical field within the permeation pathway.

Acknowledgements: Current work was founded by grants of the Deutsche Forschungsgemeinschaft to R.H. (1640/1-3) and R.H. and K.P. (1640/9-10) as well as by a fellowship to I.D. We thank Kerstin Neuwinger (Würzburg) for expert technical assistance, and Irene Marten (Hannover), Benoît Lacombe, Hervé Sentenac, Jean-Baptiste Thibaud (Montpellier) as well as Gerald Schönknecht (Würzburg) for helpful discussions and comments on the manuscript.

References

[1] Anderson, J.A., Huprikar, S.S., Kochian, L.V., Lucas, W.J. and Gaber, R.F. (1992) Proc. Natl. Acad. Sci. USA 89, 3736–3740.
[2] Schachtman, D.P., Schroeder, J.I., Lucas, W.J., Anderson, J.A. and Gaber, R.F. (1992) Science 258, 1645–1658.
[3] Sentenac, H., Bonneaud, N., Minet, M., Lacroute, F., Salmon, J.M., Gaymard, F. and Grignon, C. (1992) Science 256, 663–665.
[4] Bertl, A., Anderson, J.A., Slayman, C.L., Sentenac, H. and Gaber, R.F. (1994) Folia Microbiol. (Prague) 39, 507–509.
[5] Véry, A.A., Bosseux, C., Gaymard, F., Sentenac, H. and Thibaud, J.B. (1994) Pflügers Arch. 428, 422–424.
[6] Bertl, A., Anderson, J.A., Salyman, C.L. and Gaber, R.F. (1995) Proc. Natl. Acad. Sci. USA 92, 2701–2705.
[7] Cao, Y., Ward, J.M., Kelly, W.B., Ichida, A.M., Gaber, R.F., Anderson, J.A., Uozumi, N., Schroeder, J.I. and Crawford, N. (1995) Plant Physiol. 109, 1093–1106.
[8] Hedrich, R., Moran, O., Conti, F., Busch, H., Becker, D., Gambale, F., Dreyer, I., Küch, A., Neuwinger, K. and Palme, K. (1995) Eur. Biophys. J. 24, 107–115.
[9] Hoshi, T. (1995) J. Gen. Physiol. 105, 309–328.
[10] Müller-Röber, B., Ellenberg, J., Provart, N., Willmitzer, L., Busch, H., Becker, D., Dietrich, P., Hoth, S. and Hedrich, R. (1995) EMBO J. 14, 2409–2416.
[11] Véry, A.A., Gaymard, F., Bosseux, C., Sentenac, H. and Thibaud, J.B. (1995) Plant J. 7, 321–332.
[12] Gaymard, F., Cerutti, M., Horeau, C., Lemaillet, G., Urbach, S., Ravallec, M., Devauchelle, G., Sentenac, H. and Thibaud, J.B. (1996) J. Biol. Chem. 271, 22863–22870.
[13] Ketchum, K.A. and Slayman, C.W. (1996) FEBS Lett. 378, 19–26.
[14] Marten, I., Gaymard, F., Lemaillet, G., Thibaud, J.B., Sentenac, H. and Hedrich, R. (1996) FEBS Lett. 380, 229–232.
[15] Zimmermann, S., Talke, I., Ehrhardt, T., Nast, G. and Müller-Röber, B. (1998) Plant Physiol. 116, 879–890.
[16] Durell, S.R. and Guy, H.R. (1996) Neuropharmacology 35, 761–773.
[17] Chandy, K.G. and Gutman, G.A. (1994) in: Handbook of Receptors and Channels (North, R.A., Ed.), pp. 1–71, CRC Press, Boca Raton, FL.
[18] Hedrich, R. and Dietrich, P. (1996) Bot. Acta 109, 94–101.
[19] Dreyer, I., Antunes, S., Hoshi, T., Müller-Röber, B., Palme, K., Pongs, O., Reintanz, B. and Hedrich, R. (1997) Biophys. J. 72, 2143–2150.
[20] Daram, P., Urbach, S., Gaymard, F., Sentenac, H. and Chérel, I. (1997) EMBO J. 16, 3455–3463.
[21] Ludwig, J., Owen, D. and Pongs, O. (1997) EMBO J. 16, 6337–6345.
[22] Hoth, S., Dreyer, I. and Hedrich, R. (1997) J. Exp. Bot. 48, 415–420.
[23] Marten, I. and Hoshi, T. (1997) Proc. Natl. Acad. Sci. USA 94, 3448–3453.
[24] Becker, D., Dreyer, I., Hoth, S., Reid, J.D., Busch, H., Lehnen, M., Palme, K. and Hedrich, R. (1996) Proc. Natl. Acad. Sci. USA 93, 8123–8128.
[25] Uozumi, N., Gassmann, W., Cao, Y. and Schroeder, J.I. (1995) J. Biol. Chem. 270, 24276–24281.
[26] Ichida, A.M. and Schroeder, J.I. (1996) J. Membrane Biol. 151, 53–62.
[27] Nakamura, R.I., Anderson, J.A. and Gaber, R.F. (1997) J. Biol. Chem. 272, 1011–1018.
[28] Hoth, S., Dreyer, I., Dietrich, P., Becker, D., Müller-Röber, B. and Hedrich, R. (1997) Proc. Natl. Acad. Sci. USA 94, 4806–4810.
[29] Doyle, D.A., Cabral, J.M., Pfuetzner, R.A., Kuo, A., Gulbis, J.M., Cohen, S.L., Chait, B.T. and MacKinnon, R. (1998) Science 280, 69–77.
[30] Woodhull, A.M. (1973) J. Gen. Physiol. 61, 687–708.
[31] Liman, E.R., Tytgat, J. and Hess, P. (1992) Neuron 9, 861–871.
[32] Dietrich, P., Dreyer, I., Wiesner, P. and Hedrich, R. (1998) Planta 205, 277–287.

[33] Hoshi, T., Zagotta, W.N. and Aldrich, R.W. (1991) Neuron 7, 547–556.
[34] López-Barneo, J., Hoshi, T., Heinemann, S.H. and Aldrich, R.W. (1993) Receptors Channels 1, 61–71.
[35] De Biasi, M., Hartmann, H.A., Drewe, J.A., Taglialatela, M., Brown, A.M. and Kirsch, G.E. (1993) Pflugers Arch. 422, 354–363.
[36] Choi, K.L., Aldrich, R.W. and Yellen, G. (1991) Proc. Natl. Acad. Sci. USA 88, 5092–5095.
[37] Glasstone, S., Laidler, K.J. and Eyring, H. (1941) The Theory of Rate Processes, McGraw-Hill, New York.